Chern number in the Kitaev honeycomb lattice model

Author: Pere Tomas Prats ptomaspr7@alumnes.ub.edu
Facultat de Física, Universitat de Barcelona, Diagonal 645, 08028 Barcelona, Spain.

Advisor: Sofyan Iblisdir, iblisdir@fqa.ub.edu

Abstract: We study a topological invariant in the 2D Kitaev honeycomb model: the Chern number. This model consists of a spin $\frac{1}{2}$ hexagonal lattice that can be divided into two triangular sublattices. By applying an external perturbation we can induce a non-trivial phase for some coupling configurations that yields a non-zero Chern number. First we set a theoretical basis in order to understand the results. Then we study how different parameters affect the Chern number. More exactly; finite-size effects, an external perturbation, different coupling configurations and strengths.We will see how each of these variations change the Chern number.
Keywords: Theoretical physics, condensed matter, topological phases.
SDGs: Educació de qualitat

I. Introduction

Topology is the branch of mathematics that studies geometric properties preserved under continuous deformations. The classical example is to think of a doughnut and a mug as topologically equivalent as they have the same number of holes so you can deform one into another; however, if you try to do it with a sphere you cannot, as you would have to cut it somewhere. The interest physicists have had in topology was limited until the 1980's when topological considerations were used to describe the integer quantum Hall effect [1] [2] and the fractional quantum Hall effect [3]. Later on, Haldane presented a model [4] in which topology played a central role. However, the boom in the study of topology of quantum systems began in the 2000's, with the theoretical discovery of a 2D quantum spin Hall insulator phase [5].

Topological phases of matter are phase transitions that cannot be explained through Landau's theory of phase transitions. The physical properties of these phases can not be explained locally, as they emerge as consequences of topological considerations of the system as a whole. These phases are characterised by topological invariants. These invariants are similar to Landau local order parameters but the key difference is that they are discrete. That means that if the system experiences some continuous transformation, this parameter will remain the same unless the system undergoes a phase transition. In this work we are interested in the study of a particular topological invariant in the Kitaev honeycomb model: the Chern number.

This document is organized as follows. In Section II, we will introduce the Berry phase and its relation to the Chern number. After that, in Section III, we are going to introduce the Kitaev honeycomb model. Then we will show our simulation and results in Section IV before the conclusions in Section V.

II. Berry phase and the Chern number

Let $\sum_{\mathbf{q}} \mathcal{H}(\mathbf{q})$ denote the Hamiltonian of some translational invariant system in momentum representation. Then the Berry connection [6] is defined as

$$\begin{aligned}\Gamma^n(\mathbf{q}) &= i\,\langle e^{i\phi_n(\mathbf{q})}u_n(\mathbf{q})|\partial_{\mathbf{q}}e^{i\phi_n(\mathbf{q})}u_n(\mathbf{q})\rangle \\ &= i\,\langle u_n(\mathbf{q})|\partial_{\mathbf{q}}u_n(\mathbf{q})\rangle - \partial_{\mathbf{q}}\phi_n(\mathbf{q}),\end{aligned} \tag{1}$$

where $|e^{i\phi_n(\mathbf{q})}u_n(\mathbf{q})\rangle$ is the n-th eigenstate of the Hamiltonian. The Berry connection measures how $|e^{i\phi_n(\mathbf{q})}u_n(\mathbf{q})\rangle$ changes with $\mathbf{q}$. The "field strength" of the Berry connection is defined as

$$\mathcal{F}^n_{ij}(\mathbf{q}) = \partial_{q_i}\Gamma^n_{q_j} - \partial_{q_j}\Gamma^n_{q_i}.$$

And the Berry phase as

$$\oint dq \cdot \Gamma^n(\mathbf{q}).$$

In essence, the Berry phase is a parallel transport of the eigenstate $e^{i\phi_n(\mathbf{q})}\,|u_n(\mathbf{q})\rangle$ through a closed path. The first Chern number of the n-th band is defined as its Berry phase alongside the first Brillouin zone (BZ) divided by 2π [6]

$$Ch^n_1 = \frac{1}{2\pi}\int_{BZ} dq_x dq_y \cdot \mathcal{F}^n_{xy}(\mathbf{q}) = \frac{1}{2\pi}\oint_{BZ}\Gamma^n(\mathbf{q})dq, \tag{2}$$

The second equality comes from Stokes theorem. The first Chern number gives information on how the Berry phase "curls" in the BZ.

If it helps the reader, we can draw a parallel between the Berry connection and the relativistic form of electromagnetism (EM) [7]. If we consider the Berry connection as our gauge potential, the electric and magnetic fields are contained in the field strength. This analogy is quite useful as we can translate our knowledge from EM to the study of topological phases. However, we need to keep in mind that we are not operating in the physical space, but rather in the momentum space.

III. The Kitaev honeycomb model

The Kitaev honeycomb model [8] is defined as an hexagonal lattice of spin-$\frac{1}{2}$ fermions that can be divided into two triangular sublattices as shown in fig.(1). Nearest-neighbour interactions can be divided into three types depending on their direction as shown in fig.(2). The Hamiltonian of this model is

$$\mathcal{H} = -J_x \sum_{x-links} \sigma_j^x \sigma_k^x - J_y \sum_{y-links} \sigma_j^y \sigma_k^y - J_z \sum_{z-links} \sigma_j^z \sigma_k^z. \tag{3}$$

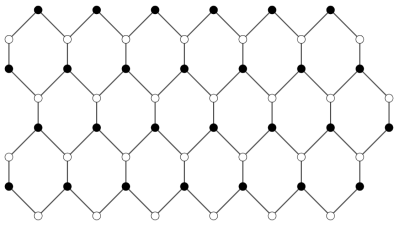

FIG. 1: Honeycomb lattice. Black and white vertices show the two different sublattices.

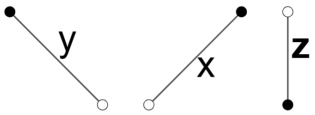

FIG. 2: Type of bonds.

In (3) we have chosen an orientation where j belongs to the white dotted sublattice and k belongs to the black dotted sublattice.

We are going to present a mapping to Majorana fermions that solve the Hamiltonian (3). Given a set of labels $\mathcal{L} = \{1 \dots L\}$, Majorana fermions are operators that satisfy the following properties.

$$\varphi_\alpha = \varphi_\alpha^\dagger, \quad \{\varphi_\alpha, \varphi_\beta\} = 2\delta_{\alpha\beta}\mathcal{I} \quad \forall \alpha, \beta \in \mathcal{L}.$$

We associate four Majorana fermions with each vertex s of the honeycomb lattice $\{b_s^x, b_s^y, b_s^z, c_s\}$. The operators b_s^x, b_s^y, b_s^z are respectively associated with the x-link, the y-link, and the z-link sticking out of vertex s. We observe that the operators $\tilde{\sigma}_s^\alpha = i b_s^\alpha c_s$, $\alpha \in \{x, y, z\}$ constitute a (representation of the) algebra of Pauli matrices. The substitution $\sigma_s^\alpha \to \tilde{\sigma}_s^\alpha$ for all vertex of the honeycomb lattice maps the spin Hamiltonian (3) to the following Majorana fermion Hamiltonian

$$\tilde{\mathcal{H}} = \frac{i}{4} \sum_{j,k} \hat{A}_{jk} c_j c_k, \tag{4}$$

where $\hat{A}_{jk} = 2J_{\alpha jk}\hat{u}_{jk}$ if j and k are linked, otherwise $\hat{A}_{jk} = 0$. For each link of the lattice (j, k), the operator $\hat{u}_{jk}$ is defined as $i b_j^\alpha b_k^\alpha$, where α denotes the type of link (x, y, z). These operators commute with $\tilde{\mathcal{H}}$, with one another, and satisfy $\hat{u}_{jk} = -\hat{u}_{kj}$. Their eigenvalues are $u_{jk} = \pm 1$.

Another important operator is $\tilde{W}_p = \prod_{(j,k)\in p} \hat{u}_{jk}$, which is the product of every $\hat{u}_{jk}$ around the boundary of an hexagon p. This operator also commutes with the Hamiltonian and the corresponding eigenvalue is the product of the eigenvalues of $\hat{u}_{jk}$. This value is also interpreted as the magnetic flux through the hexagon p. If $w_p = -1$ we say that this hexagon carries a vortex. The total Hilbert space can be written as a direct sum of what we call sectors, represented by $\mathbf{w}$. A sector is a certain configuration of all possible w_p values. We can also divide the Hamiltonian into these sectors as it commutes with the magnetic flux operator, $\tilde{\mathcal{H}} = \bigoplus_{\mathbf{w}} \tilde{\mathcal{H}}_{\mathbf{w}}$. In each sector $\mathbf{w}$, the Hamiltonian $\tilde{\mathcal{H}}_{\mathbf{w}}$ is quadratic and thus solvable.

What Kitaev wanted to achieve by representing the system with Majorana fermions was not only to solve the Hamiltonian. Indeed, with this model, it is possible to get Majorana modes that could be used as topological qubits that offer some robustness against decoherence [9].

For our purposes, we need to identify the sector that contains the ground state. Using a result by Lieb [10] we can prove that the ground state of (4) is given when $w_p = 1 \quad \forall p$. This sector is called the vortex free configuration. This also means a change of sign of any J_α does not change the ground state because it can be reverted by setting all the u_{jk} in the α direction to -1. Also interchanging the value of the coupling parameter of two directions leaves the system the same because it is equivalent to rotating the whole system 120^{o} or 240^{o} degrees. This rotation does not change the system as it has rotational symmetry.

The vortex free configuration possesses translational symmetry. This is very useful because we can perform a Fourier transformation to go to the momentum representation. The Hamiltonian in momentum space (5) is a sum of block diagonal matrices where every block is a 2×2 matrix, as shown in (6).

$$\mathcal{H} = \frac{i}{2} \sum_{\mathbf{q},\lambda,\mu} \widetilde{\mathcal{A}}_{\lambda\mu}(\mathbf{q}) a_{-\mathbf{q},\lambda} a_{\mathbf{q},\mu}. \tag{5}$$

$$i\widetilde{\mathcal{A}}(\mathbf{q}) = \begin{pmatrix} 0 & i \cdot f(\mathbf{q}) \\ -i \cdot f(\mathbf{q})^* & 0 \end{pmatrix}, \tag{6}$$

where $f(\mathbf{q}) = 2(J_x e^{i(\mathbf{q},\mathbf{n_1})} + J_y e^{i(\mathbf{q},\mathbf{n_2})} + J_z)$ and $\mathbf{q} \in$ Bz. It follows that the energy dispersion is $\epsilon(\mathbf{q}) = \pm|f(\mathbf{q})|$. We see that the relationship between the coupling parameters defines whether this spectrum is gapped or not. More specifically, if $|J_x|, |J_y|, |J_z|$ satisfy the triangle inequalities the spectrum is gapless, these configurations belong to phase B, if not we are in phase A. These phases can be represented when $J_x, J_y, J_z \geq 0$ by the diagram in fig.(3).

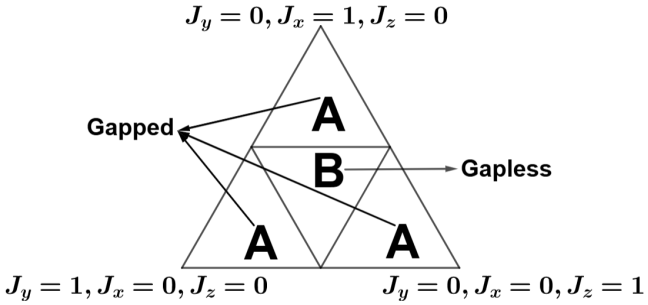

FIG. 3: Phase dependency on coupling parameters that satisfy $J_x + J_y + J_z = 1$ in the positive octant.

Non-zero values for the Chern number can be achieved by applying the following perturbation.

$$\tilde{V} = ih \sum_{m,n,o} u_{mn} c_m c_o. \tag{7}$$

In this sum, m and o are nearest-neighbours of the vertex n as shown in fig.(4). This perturbation allow us to still use the previous mathematical development as it preserves translational invariance.

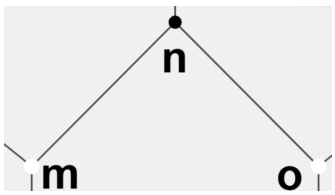

FIG. 4: Example of three contiguous vertex in the honeycomb lattice.

This perturbation modifies (6) and the energy dispersion as

$$i\widetilde{\mathcal{A}}(\mathbf{q}) = \begin{pmatrix} \Delta(\mathbf{q}) & i \cdot f(\mathbf{q}) \\ -i \cdot f(\mathbf{q})^* & -\Delta(\mathbf{q}) \end{pmatrix}, \tag{8}$$

$$\epsilon(\mathbf{q}) = \pm\sqrt{|f(\mathbf{q})|^2 + |\Delta(\mathbf{q})|^2}. \tag{9}$$

The term $\Delta(\mathbf{q}) = 4h(\sin(\mathbf{q}, \mathbf{n_1}) + \sin(\mathbf{q}, -\mathbf{n_2}) + \sin(\mathbf{q}, \mathbf{n_2} - \mathbf{n_1}))$ opens the gap in phase B.

Finally, we can compute the Chern number. From (8) we can now consider the global spectral projector in the momentum space $\widetilde{P}(\mathbf{q})$ which projects the matrix onto the occupied band subspace (those eigenstates with negative energy):

$$\widetilde{P}(\mathbf{q}) = \frac{1}{2}(\mathcal{I} - sgn(i\widetilde{\mathcal{A}}(\mathbf{q})). \tag{10}$$

The connection between $\widetilde{P}(\mathbf{q})$ and (2) is discussed in [11]. The conclusion is that the first Chern number of the n-th occupied band is computed as:

$$Ch_1^n = \frac{1}{2\pi i} \int \mathrm{Tr}\Big(\widetilde{P}(\frac{\partial \widetilde{P}}{\partial q_x}\frac{\partial \widetilde{P}}{\partial q_y} - \frac{\partial \widetilde{P}}{\partial q_y}\frac{\partial \widetilde{P}}{\partial q_x})\Big) dq_x dq_y, \tag{11}$$

we will refer to the first Chern number as just the Chern number as we will not use any other Chern number. In our case, we only have one band (see fig.(6) in Section IV) so $n = 1$. At this point, time-reversal symmetry, $\mathcal{T}$, plays an interesting role in the computation of the Chern number.

$$\mathcal{T} i\widetilde{\mathcal{A}}(\mathbf{q}) = i\widetilde{\mathcal{A}}(-\mathbf{q}) = \begin{pmatrix} -\Delta(\mathbf{q}) & if(\mathbf{q})^* \\ -if(\mathbf{q}) & \Delta(\mathbf{q}) \end{pmatrix} = -(i\widetilde{A}(\mathbf{q}))^T$$

$$\mathcal{T}\widetilde{P}(\mathbf{q}) = \widetilde{P}(-\mathbf{q}) = \frac{1}{2}[\mathcal{I} - sgn(i\widetilde{\mathcal{A}}(-\mathbf{q}))]$$
$$= \frac{1}{2}[\mathcal{I} + sgn((i\widetilde{\mathcal{A}}(\mathbf{q}))^T)]$$

If $\Delta(\mathbf{q}) = 0$, then $sgn((i\widetilde{\mathcal{A}}(\mathbf{q}))^T) = sgn(i\widetilde{\mathcal{A}}(\mathbf{q}))$ so $\widetilde{P}(-\mathbf{q}) = \mathcal{I} - \widetilde{P}(\mathbf{q})$. Because the Chern number is invariant under time-reversal symmetry when $\Delta(\mathbf{q}) = 0$ it must satisfy

$$\begin{aligned} Ch_1^1 = & \\ &= \int \frac{\mathrm{Tr}}{2\pi i}\Big(\widetilde{P}(-\mathbf{q})(\frac{\partial \widetilde{P}}{\partial(-q_x)}\frac{\partial \widetilde{P}}{\partial(-q_y)} \\ &\qquad - \frac{\partial \widetilde{P}}{\partial(-q_y)}\frac{\partial \widetilde{P}}{\partial(-q_x)})\Big) d(-q_x) d(-q_y) \\ &= \int \frac{\mathrm{Tr}}{2\pi i}\Big((\mathcal{I} - \widetilde{P}(\mathbf{q}))(\frac{\partial \widetilde{P}}{\partial q_x}\frac{\partial \widetilde{P}}{\partial q_y} - \frac{\partial \widetilde{P}}{\partial q_y}\frac{\partial \widetilde{P}}{\partial q_x})\Big) dq_x dq_y \\ &= -Ch_1^1 \\ &= 0. \end{aligned}$$

This means that to get a non-zero Chern number we need $\Delta(\mathbf{q}) \neq 0$. However, this condition is necessary but not sufficient. Kitaev proves in [8] that the Chern number in phase A is always 0 and in phase B $Ch_1^1 = sgn(h) = \pm 1$.

One of the main characteristics of these non-trivial topological phases is the presence of edge states. These states can cross the gap and they usually transport charge in quantum Hall systems. Here, Majorana fermions cannot carry charge as they are chargeless; they actually only transport thermal energy. Conformal field theory (CFT) predicts that there are edge energy currents:

$$I = \frac{\pi}{24} Ch_1^1 T^2. \tag{12}$$

Although we are not going to use this, it is important to highlight the magnitude being carried to gain insight of the system and to differentiate it from other topological phases.

IV. Simulation and Results

Our simulation begins in (8) with the unit cell and vector basis $\vec{n_1} = (\frac{1}{2}, \frac{\sqrt{3}}{2})$ and $\vec{n_2} = (-\frac{1}{2}, \frac{\sqrt{3}}{2})$ as shown in fig.(5). Before we compute the Chern number we started by representing the energy dispersion in phase B throughout the BZ to get an idea of the band structure we will work with in fig.(6). We can see two points where the gap closes in fig.(6a) with conic singularities and how the perturbation opens a gap in fig.(6b).

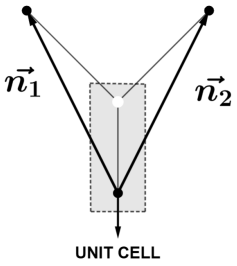

FIG. 5: Unit cell of the honeycomb lattice and real space basis vectors.

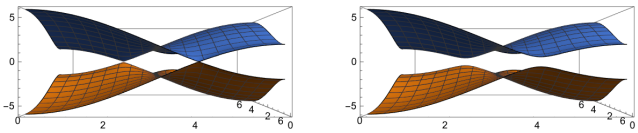

(a) (b)

FIG. 6: Band structure of phase B in the Brillouin Zone with all coupling parameters set to J=1.The perturbation is set to h=0 for (a) and h=0,055 for (b).

First, we have tested how the Chern number evolves with the perturbation for different configurations of J_x, J_y, J_z. Our results are shown in fig.(7), fig.(8) and fig.(9).

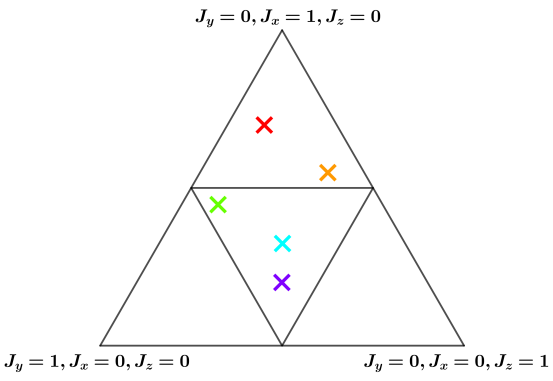

FIG. 7: Points used in fig.(8).

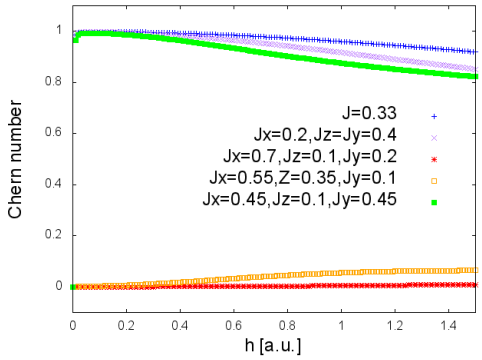

FIG. 8: Evolution of the Chern number with h for different couplings J_x, J_y, J_z with system size $2^7 \times 2^7$ points.

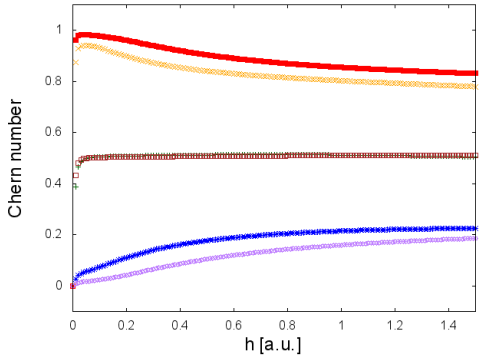

FIG. 9: Evolution of the Chern number with the perturbation for different couplings J_x, J_y, J_z. Red, brown and purple corresponds to a system size of $2^8 \times 2^8$ and orange, green and blue to a system size of $2^7 \times 2^7$. Red and orange correspond to the couplings: $J_x = 0,31$, $J_y = 0,49$, $J_z = 0,2$. Green and brown correspond to the couplings: $J_x = 0,3$, $J_y = 0,5$, $J_z = 0,2$. Blue and purple correspond to the couplings: $J_x = 0,29$, $J_y = 0,51$, $J_z = 0,2$.

In fig.(8) we observe how effective the Chern number works as a topological invariant to distinguish between phase A and phase B. If we focus on the orange and red dots or the blue and green dots in fig.(7), we see how when the coupling parameters configuration stays away from the phase transition, the Chern number becomes more robust in fig.(8). In fig.(9) we show how for two different system sizes the Chern number evolves with h in the transition between A and B phases. We observe that the Chern number still differentiates both phases until we get to the phase transition (green and brown lines). Here the Chern number is found to be $\sim 0,5$.

To see how important finite-size effects may be we can look at fig.(9) and fig.(10), where we have plotted the evolution of the Chern number when all coupling parameters are set to $J = 1$ (this configuration corresponds to the blue dot in fig.(7)) but for different system sizes.

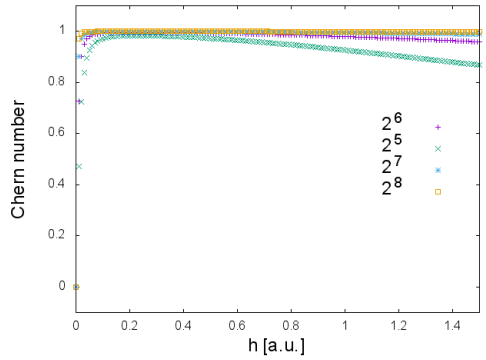

FIG. 10: Size-dependency of the Chern number in a $n \times n$ grid.

We see in both fig.(9) and fig.(10) how the bigger the system size gets the more robust the Chern number is. Finally, if we compare the blue line in fig.(8) and fig.(10) we see that the stronger the coupling parameters are, the more robust the Chern number is. This effect can be greater than finite-size effects given that in fig.(10) the purple line is closer to 1 than the blue line in fig.(8) even though the system is smaller.

V. Conclusions

In conclusion, in this work we have studied the robustness of the Chern number for the Kitaev honeycomb model in the vortex free configuration. This configuration corresponds to the ground state of the Hamiltonian (4). The vortex free configuration can be divided into phases A and B depending on the coupling parameters. Phases A are characterised by a gap in the energy dispersion when no perturbations are applied, in these phases the Chern number is always equal to 0. Phase B on the other hand, does not have a gap when the system is not perturbed and the Chern number equals ± 1 when the perturbation (7) is applied. We have studied the evolution of the Chern number with the perturbation, different coupling parameters of (3) and the size of the system. We have concluded that the Chern number is more robust when the system is bigger and the further the coupling parameters configuration is from the phase transition in fig.(7). We have also seen how stronger coupling parameters lead to more robust values of the Chern number.

Acknowledgments

First, i would like to thank my advisor Sofyan Iblisdir for introducing me to this topic and being really helpful during the meetings. I would also like to thank my friends and specially my family for supporting me throughout my degree.

[1] K. v. Klitzing, G. Dorda, and M. Pepper, "New method for high-accuracy determination of the fine-structure constant based on quantized hall resistance," *Phys. Rev. Lett.*, vol. 45, pp. 494–497, Aug 1980. [Online]. Available: https://link.aps.org/doi/10.1103/PhysRevLett.45.494

[2] D. J. Thouless, M. Kohmoto, M. P. Nightingale, and M. den Nijs, "Quantized hall conductance in a two-dimensional periodic potential," *Phys. Rev. Lett.*, vol. 49, pp. 405–408, Aug 1982. [Online]. Available: https://link.aps.org/doi/10.1103/PhysRevLett.49.405

[3] D. C. Tsui, H. L. Stormer, and A. C. Gossard, "Two-dimensional magnetotransport in the extreme quantum limit," *Phys. Rev. Lett.*, vol. 48, pp. 1559–1562, May 1982. [Online]. Available: https://link.aps.org/doi/10.1103/PhysRevLett.48.1559

[4] F. D. M. Haldane, "Model for a quantum hall effect without landau levels: Condensed-matter realization of the "parity anomaly"," *Phys. Rev. Lett.*, vol. 61, pp. 2015–2018, Oct 1988. [Online]. Available: https://link.aps.org/doi/10.1103/PhysRevLett.61.2015

[5] C. Kane, "Z 2 topological order and the quantum spin hall effect," *Physical review letters*, vol. 95, p. 146802, 10 2005.

[6] M. Sato and Y. Ando, "Topological superconductors: a review," *Reports on Progress in Physics*, vol. 80, no. 7, p. 076501, May 2017. [Online]. Available: http://dx.doi.org/10.1088/1361-6633/aa6ac7

[7] D. Tong, "Lectures on the quantum hall effect," 2016. [Online]. Available: https://arxiv.org/abs/1606.06687

[8] A. Kitaev, "Anyons in an exactly solved model and beyond," *Annals of Physics*, vol. 321, no. 1, p. 2–111, Jan. 2006. [Online]. Available: http://dx.doi.org/10.1016/j.aop.2005.10.005

[9] ——, "Fault-tolerant quantum computation by anyons," *Annals of Physics*, vol. 303, no. 1, p. 2–30, Jan. 2003. [Online]. Available: http://dx.doi.org/10.1016/S0003-4916(02)00018-0

[10] E. H. Lieb, "Flux phase of the half-filled band," *Physical Review Letters*, vol. 73, no. 16, p. 2158–2161, Oct. 1994. [Online]. Available: http://dx.doi.org/10.1103/PhysRevLett.73.2158

[11] J. E. Avron, R. Seiler, and B. Simon, "Homotopy and quantization in condensed matter physics," *Phys. Rev. Lett.*, vol. 51, pp. 51–53, Jul 1983. [Online]. Available: https://link.aps.org/doi/10.1103/PhysRevLett.51.51

El número de Chern en el model de malla hexagonal de Kitaev

Author: Pere Tomas Prats ptomaspr7@alumnes.ub.edu
Facultat de Física, Universitat de Barcelona, Diagonal 645, 08028 Barcelona, Spain.

Advisor: Sofyan Iblisdir, iblisdir@fqa.ub.edu

Resum: En aquest treball hem estudiat com evoluciona un invariant topològic del model honeycomb de Kitaev: el nombre de Chern. Basant-nos en el seu paper de 2006 hem calculat el valor del número de Chern amb l'ajuda d'un codi en què hem treballat en l'espai de Fock de Majorana en espai de moments. Hem vist com aquest invariant topològic evoluciona en funció d'una pertorbació, de la dimensió del sistema i dels paràmetres d'enllaç entre els vèrtex de la malla.
Paraules clau: Física teòrica, matèria condensada, Fases topològiques.
ODSs: Educació de qualitat.

Objectius de Desenvolupament Sostenible (ODSs o SDGs)

1. Fi de la es desigualtats		10. Reducció de les desigualtats	
2. Fam zero		11. Ciutats i comunitats sostenibles	
3. Salut i benestar		12. Consum i producció responsables	
4. Educació de qualitat	X	13. Acció climàtica	
5. Igualtat de gènere		14. Vida submarina	
6. Aigua neta i sanejament		15. Vida terrestre	
7. Energia neta i sostenible		16. Pau, justícia i institucions sòlides	
8. Treball digne i creixement econòmic		17. Aliança pels objectius	
9. Indústria, innovació, infraestructures			